Impact of Subgrid-scale Orography on Equatorial Angular Momentum Budget and the Cold Surges in a General Circulation Model

Sylvain Mailler * François Lott

Laboratoire de Météorologie Dynamique (IPSL) / CNRS / ENPC, Paris, France

ABSTRACT

The dynamical relations between Equatorial Atmospheric Angular Momentum (EAAM), equatorial mountain torques and cold surges are analyzed in a General Circulation Model (GCM). First we show that the global EAAM budget is well closed in the GCM, and much better than in the NCEP reanalysis. We then confirm that the equatorial torques due to the Tibetan plateau, the Rockies and the Andes are well related to the cold surges developing over East Asia, North America, and South America respectively. For all these mountains, a peak in the equatorial mountain torque components precedes by few days the development of a cold surge, confirming that the cold surges "preconditioning" is dynamically driven by large-scale mountains.

We also analyze the contribution of the subgrid scale orography (SSO) parameterizations and find that they contribute substantially to the torques. In experiments where these parameterizations are almost entirely reduced over a given massif we find that the explicit pressure torques produced by that massif largely compensate the reduction in the parameterized torques. On the one hand, this proves that the explicitly resolved equatorial mountain torques are effective dynamical drivers of the flow dynamics, since they are enhanced when a parameterized force is reduced. On the other hand, this shows that the cold surges can be captured in GCMs, provided that the synoptic conditions prior to their onset are realistic. The compensation between torques is nevertheless not complete and some weakening of the cold surges is found when the parameterized mountain torques are reduced.

1. Introduction

Cold surges are synoptic-scale meteorological events that occur on the eastern flanks of large-scale mountain massifs in winter. They are very pronounced east of the Tibetan Plateau, the Rockies, and the Andes yielding to the East Asian, North American, and South American cold surges respectively. In these three regions, they deeply affect the local climate and agriculture bringing extremely cold temperature in East-Asia (Zhang et al. (1997); Chen et al. (2002)), North America (Konrad II (1996); Schultz et al. (1998); Portis et al. (2006); Shafer and Steenburgh (2008)), and South America (Marengo et al. (1997)). In these three regions, the origin of the cold surges can be traced back from anticyclonic anomalies in the lower layers of the midlatitude troposphere poleward of the massif, which produce a cold tongue about 2000 m thick above the surface (Garreaud (2001)). As this cold anomaly is associated with high surface pressure, it is dynamically influenced by the topography and tends to move equatorward east of the massif, following a mechanism described in Mailler and Lott (2010).

When a cold surge enters into the subtropics, its impact on the temperature loses intensity through interactions with warmer surfaces, but it can still produce substantial effects (Garreaud (2001)). In eastern Asia, this meridional propagation towards the tropics affects the winter monsoon convection over the Southern China Sea (Mailler and Lott (2009)), in North America it makes that the most intense cold surges produce freezing temperatures down to Florida and Eastern Mexico (Pérez García (1996); Schultz et al. (1997)). In South America, this equatorward propagation has a speed of $20\,\mathrm{ms}^{-1}$ up to the Peruvian Amazon (Espinoza et al. (2012)) and impacts the onset of the wet season over Amazonia (Li and Fu (2006)a).

From a more global point of view, the East Asian and North American cold surges are among the dominant modes of variability of the winter climate in the northern hemisphere (Hsu and Wallace (1985)), they also generate meridional heat fluxes contributing to about 10% of the global energy transport between the midlatitudes and the tropics (Garreaud (2001)). Also, the East Asian cold surges are influenced by major modes of climate variability like the Arctic oscillation (Woo et al. (2012); Park et al. (2011);

Jeong and Ho (2005)), and the Madden-Julian oscillation (Park et al. (2010); Jeong et al. (2005)).

The large-scale circulation patterns that interact dynamically with mountains to initiate cold-surges as well as their subsequent developments have been described by many authors. For the case of the South American cold surges, a ridge first develops over the Western Pacific, travels eastward to the southern tip of South America where it begins to be deviated dynamically northeastward by the Andes (Garreaud (1999, 2000); Vera and Vigliarolo (2000); Marengo et al. (2002); Pezza and Ambrizzi (2005)). This equatorward deviation, which is referred to as preconditionning in Mailler and Lott (2010), is common to all the cold surges. In subsequent stages, linear wave propagation along the topographic gradient (topographic or Kelvin waves) and non-linear processes (cold advection, tropical convection acting as a positive feedback) help the cold surge to intensify while still propagating along the mountain slope (see Reason (1994); Colle and Mass (1995); Schultz et al. (1997); Compo et al. (1999), for the case of the North American cold surges).

Although the intrusion of cold anticyclonic air into subtropical latitudes can occur in the absence of mountains (Sprenger et al. (2013)), the mountain forcing dynamically amplifies and helps to focus them regionally (Garreaud (2001)). In a f-plane geometry, this dynamical forcing can be measured as the integral over the mountain surface of the pressure force exerted on the atmosphere and of the surface stresses due to the boundary layer and SSO parameterizations. In the horizontal direction, this forcing is a vector with two horizontal components, a mountain drag that is essentially opposite to the low level wind and a mountain lift that is essentially perpendicular to it (e.g. Lott (1995)). In the cases of the Eastern Asia, North American and South American cold surges, the mountain ranges have almost planetary scales and the sphericity of the earth needs to be taken into account. To evaluate the dynamical contribution of the mountains, one therefore need to adopt the dynamical framework of the equatorial atmospheric angular momentum (EAAM) budget. In this framework, the forcing vector becomes the the Equatorial mountain torque (EMT), which also has two components, one along each equatorial axis, and each large scale massive contribute individually to it. It is in this framework that Mailler and Lott (2010) have shown that maxima in the first component of the EMT due to the Tibetan plateau are associated with a strengthening of the Siberian anticyclone and followed about two days later by a cold surge of about 8 K in eastern China. This drop in temperature is associated with a surface pressure surge of about 10 hPa. This high pressure then generates a negative signal on the second component of the EMT. They found similar results for North America and South America and also proved, by using a simplified mechanistic model with a spherical surface, that these relations do not simply reflect a passive correlation between the surface pressure and the mountain elevation. In this simplified mechanistic model, surface stresses are deposited into the surface layer of a spherical quasi-geotrophic atmosphere, and, when these stresses give EMT values that are realistic in amplitude and location the model produces realistic cold surges.

The observational results in Mailler and Lott (2010) have been obtained with the NCEP reanalysis, which does not provide an accurate closure of the AAM budget, neither in its axial component (Lott et al. 2005) nor in its equatorial components (Feldstein 2006). On the contrary, we know that the Laboratoire de Meteorologie Dynamique model with zoom (the LMDz) GCM closes well the axial AAM budget (Lott et al. 2005; Lebonnois et al. 2010), and also has a good closure of the EAAM budget at subdiurnal periodicities (De Viron et al. 2005). We can therefore use this model to confirm the results in Mailler and Lott (2010) after verification that LMDz (i) closes the EAAM budget at longer time scales, and (ii) reproduces the relation between the local torques and the cold surges. This will also permit to verify that pressure torques and parameterized torques can in good part be treated on the same footing, i.e. to propose a quantitative way to test mountain representation in models.

In this context, another motivation is to understand the contribution of the SSO parameterizations to the synoptic scale flow (some aspects of this problem are discussed in Aebischer and Schar (1998); Martin and Lott (2007)). Although not often done, this can become an issue in the atmospheric models that are included in the Earth System Models to study the climate change, because in them, the coarse resolutions often used can make the SSO parameterizations contribute substantially. Since these models are also used to study the regionalisation of the climate change (Giorgi et al. 2009), their representation of regional synoptic scale phenomena like the cold surges needs to be realistic.

The purpose of this paper is to re-examine the dynamical link between EMT and cold surges in a model that closes the EAAM budget. First, it will be shown that the LMDz GCM closes the EAAM budget and second that it reproduces the dynamical links between the EMT and cold surges. Finally, we will examine the contribution of the subgrid-scale orographic (SSO) parameterizations to the EAAM budget in LMDz and to the dynamics of the cold surges.

The plan of the paper is as follows. Section 2 describes the data and methods used. Section 3 analyzes the budget of the equatorial AAM in LMDz. Section 4 provides an analysis of the Tibetan plateau contributions to the EMT and the relation with the East Asian cold surges. Section 5 treats the case of the Rockies and the Andes. In both sections 4 and 5, the contribution of the parameterized

torques is also discussed. Section 6 presents the sensitivity of our results to these parameterized torques by making three sensitivity tests where the SSO parameterizations are suppressed over the Tibetan plateau, the Rockies and the Andes. Section 7 concludes and discusses the results obtained in the context of the simulation of cold surges and of the representation of mountains in large-scale models.

2. Data and methods

a. Model description

The model data used in this paper are derived from simulations done with the LMDz gridpoint GCM version 4 described in Hourdin et al. (2006), and which closes accurately the axial AAM budget (Lott et al. 2005). In all simulations the horizontal resolution is $3.75° \times 2.5°$, and there are 19 levels in the vertical, most of them in the troposphere. Although we have chosen a coarse resolution to match the configurations used to build the IPSL-ESM for CMIP5 (Dufresne 2013), we will see that this coarse resolution allows the model to represent the cold surge preconditionning and its relation with the EMT. At the lower boundary, the model is forced by sea surface temperatures and sea ice cover that vary along a mean climatological annual cycle.

In the LMDz model, the impact of subgrid-scale orography (SSO) is represented in three distinct ways. First, in the boundary layer scheme, the roughness length is increased over mountains to represent the increase in turbulence produced by narrow hills (Belcher and Wood (1996)) and the increasing factor is directly proportional to the SSO slope time its standard deviation. Second, the mesoscale impact of SSO is taken into account following Lott and Miller (1997), where gravity waves breaking and low level blocked flow drags are parameterized. As this scheme mainly acts at low levels, and competes with the increased boundary layer drag there, we will combine them into a single SSO drag. Here we deliberately used the term SSO drag, because both parameterizations applies tendencies on the wind essentially opposite to the low level flow. This contrasts to the third way we represent SSO, which consists in taking into account the sheltering of air in mountain valleys. Following Lott (1999), this is represented by applying tendencies on the wind essentially perpendicular to the flow, and we use the term SSO lift. We know from this paper but also from Mailler and Lott (2009), that it is almost equivalent to rising the lowest model level, at least in the quasi-geostrophic framework. It has been shown by Lott (1999) that the inclusion of a SSO lift in LMDz improve the representation of the steady planetary waves in the model by enhancing vortex stretching above the major mountain massifs

To address the significance of these parameterizations on the local climate, four 30 year simulations have been performed. One is a control simulation, and the other three are simulations where the SSO parameterizations are set to zero over (i) the Tibetan Plateau ([20N;60N]×[60E;110E]), (ii) the Rockies ([180W;90W]×[15N;70N]), and (iii) the Andes ([90W;60W]×[50S;10N]). Note that to neutralize these SSO parameterizations over the corresponding sector we just put to zero the SSO parameters when preparing the experiment. To avoid a too sharp transition, the SSO parameters are also multiplied by a smooth taper function in a buffer zone of 15° in latitude and longitude around the domains of interest. Finally, to validate our results, we use 30 years (1979-2008) of daily data from the NCEP reanalysis (Kalnay et al. 1996).

b. EAAM budget and torques

Most of our diagnostics are based on the EAAM budget equations given for instance in Feldstein (2006):

$$\frac{\mathrm{d}M_1}{\mathrm{d}t} = \Omega M_{r2} + \underbrace{T_{M1} + T_{d1} + T_{l1}}_{T_{t1}}, \tag{1a}$$

$$\frac{\mathrm{d}M_2}{\mathrm{d}t} = -\Omega M_{r1} + \underbrace{T_{M2} + T_{d2} + T_{l2}}_{T_{t2}}. \tag{1b}$$

In these equations, $M_1 = M_{r1} + M_{m1}$ is the total atmospheric angular momentum along the first equatorial axis (the equatorial axis at the longitude of Greenwich), where M_{r1} and M_{m1} are the wind and mass angular momentum along the same axis. M_2, M_{r2}, and M_{m2} are the corresponding components along the second equatorial axis which crosses the Equator at 90°E longitude (see Table 1 for the integral expression of these variables). Still in (1a)-(1b), the total torques T_{t1} and T_{t2} are each split in three terms, the first T_{M1} and T_{M2} are the two equatorial components of the mountain torque explicitly solved by the model, the second T_{d1} and T_{d2} are the equatorial torques due to the SSO drag (turbulent + mesoscale) and the third T_{l1} and T_{l2} are the torques due to the SSO lift. The expressions for all these terms are given in Table 1. Finally, the torques as well as the time derivative of the angular momenta will be expressed in Hadleys, with $1\,\mathrm{Ha}=10^{18}\,\mathrm{kg\,m^{-2}\,s^{-2}}$.

Concerning the torques, the equatorial components have been evaluated both globally, for the analysis of the global EAAM budget, and regionally for the Tibetan Plateau, the Rockies and the Andes. The regional contributions are computed by restricting the integrations to appropriate regions largely including the considered mountain range: [20N;60N]×[60E;110E] for the Tibetan Plateau, [180W;90W]×[15N;70 for the Rockies, and [90W;60W]×[50S;10N] for the Andes. For the Andes and the Rockies, a rotation of the equatorial axes is also performed so that the second equatorial axis crosses the Equator at the longitude of the centre of the

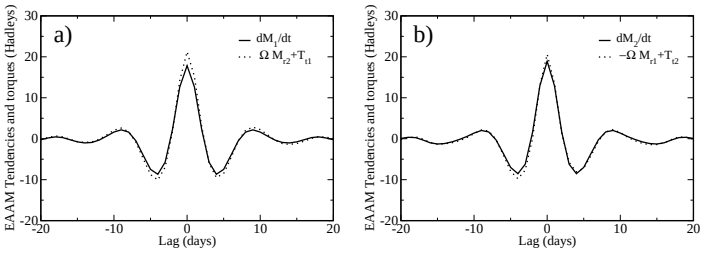

(a) (b)

FIG. 1. (a) Regression of both sides of (Eq. 1a) keyed to the left-hand side of the equation, $\frac{\mathrm{d}M_1}{\mathrm{d}t}$: $\frac{\mathrm{d}M_1}{\mathrm{d}t}$ (gray), and $\Omega M_{r2} + T_{t1}$ (mixed double); et (b) regressions of both sides of (1b) keyed to left-hand side $\frac{\mathrm{d}M_2}{\mathrm{d}t}$: $\frac{\mathrm{d}M_2}{\mathrm{d}t}$ (gray), and $-\Omega M_{r1} + T_{t2}$ (mixed double). the x-axis is the time lag in days, the y-axis is in Ha.

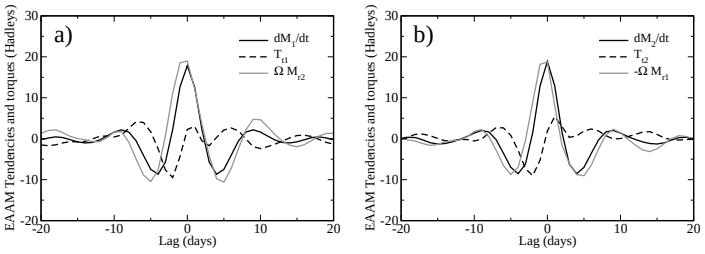

(a) (b)

FIG. 2. (a) Regressions of the most important terms of (1a) keyed to the left-hand side $\frac{\mathrm{d}M_1}{\mathrm{d}t}$: $\frac{\mathrm{d}M_1}{\mathrm{d}t}$ (gray), total torque applied to the atmosphere T_{t1} (dashed); and ΩM_{r2} (mixed), and (b) regression of the principal terms of (1b) keyed to the left-hand side $\frac{\mathrm{d}M_2}{\mathrm{d}t}$: $\frac{\mathrm{d}M_2}{\mathrm{d}t}$ (gray), T_{t1} (dashed) and $-\Omega M_{r1}$ (mixed). The x-axis is the time lag in days, the y-axis is in Ha

considered mountain range (see Mailler and Lott (2010) for more details).

3. EAAM budget in LMDz

To measure the realism of the EAAM variations in our model we follow Feldstein (2006) and, for the first axis, evaluate the auto-regression of $\frac{\mathrm{d}M_1}{\mathrm{d}t}$ on itself (Fig. 1a). First, we find that the auto-regression of $\frac{\mathrm{d}M_1}{\mathrm{d}t}$ is very similar to that found in reanalysis (see Fig. 2c in Feldstein (2006)) and presents the 8-10 day quasi-periodicity already found by Bell (1994). The maximal amplitude of 20 Ha in Fig. 1a is also in agreement with the value obtained by Feldstein (2006), and comparable behaviours are found for the second axis (e.g. $\frac{\mathrm{d}M_2}{\mathrm{d}t}$ in Eq. 1b and Fig. 1b). As we know from Bell (1994) and Feldstein (2006) that this quasi periodicity in the two EAAM components is primarily related to the westward propagation of free planetary Rossby waves, we can attribute the realism of our result to the fact that the planetary scale free Rossby waves are realistic in the LMDz-GCM (Lott et al. (2009)).

To evaluate the accuracy of the budget closure, we also evaluate the regression of the forcing term $\Omega M_{r2} + T_{t_1}$ on the EAAM tendency $\frac{dM_1}{dt}$, e.g the right against the left hand side term in Eq 1a . We found an excellent correspondence with the auto-regression of $\frac{dM_1}{dt}$ (Fig. 1a), and the same is true if we repeat the comparison for the second axis (see Fig. 1b). These excellent closures are quite noticeable since Feldstein (2006) reports important discrepancies between the same terms in the NCEP reanalysis whereas Egger et al. (2007) mention that in general GCMs do not close well the 3 components of the AAM budget. If we complete our results here by the sub-diurnal periodicities analyzed in De Viron et al. (2005), or by the daily axial component in Lott et al. (2005), we can conclude that LMDz closes well the budget of the complete AAM vector.

Fig. 2a splits the contribution of the total torques T_{t1} and of the Coriolis term ΩM_{r2} to the EAAM tendency $\frac{\mathrm{d}M_1}{\mathrm{d}t}$. It shows that $\frac{\mathrm{d}M_1}{\mathrm{d}t}$ is primarily driven by the Coriolis term ΩM_{r2}, the contribution of the total torque T_{t1} being smaller and in opposition (Fig. 2a). Similar results are found for the second axis (Fig. 2b). The variations of the equatorial angular momentum are therefore more correlated to the rotation term $-\mathbf{\Omega} \times \mathbf{M}_r$ than to the total torque $\mathbf{T}_t$ applied to the atmosphere. This is consistent with the fact that during their propagation free Rossby waves induce changes in EAAM that are equilibrated by the Coriolis torque, a process that can occur even in the absence of mountains (Bell 1994; Feldstein 2003). Despite this, we see that the mountain torques play a significant role, essentially prior to the peaks in EAAM tendency, introducing a delay between the Coriolis torque and the corresponding EAAM tendency.

The fact that EAAM budgets are not well closed in reanalysis or models in part follows that there is a large cancellation between the terms that force the changes in the EAAM vector $\mathbf{M}$, e.g. between the Coriolis term $-\mathbf{\Omega} \times \mathbf{M}_r$ and the total torque $\mathbf{T}_t$. To make this clear Fig. 3 shows the different terms of the EAAM budget in Eq. (1a) keyed to the explicit torque T_{M1} (see also Fig. 6 in Egger and Hoinka (2002)). The most striking effect is the compensation between ΩM_{r2} and T_{t1}. This compensation in fact dominates the global budget: the peak value for the regression of ΩM_{r2} on T_{t1} in Fig. 3a is almost three times larger then the peak value found when the regression is keyed to $\frac{dM_1}{dt}$, and this is consistent with the fact that (i) the variances of ΩM_{r2} and T_{t1} (65 Ha and 63 Ha respectively) are much larger than that of $\frac{\mathrm{d}M1}{\mathrm{d}dt}$ (21 Ha), and (ii) that these two series are largely anticorrelated (with a correlation coefficient of -0.91). This compensation also occurs between T_{t2} and $-\Omega M_{r1}$ in Eq. (1b).

From these large cancellation it is quite natural that small errors on the pressure or on the winds, yielding small

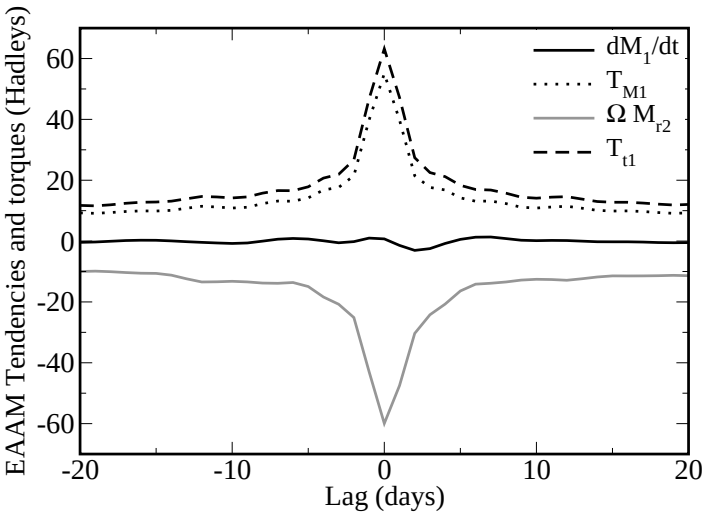

FIG. 3. regression of the main terms of (1a) keyed to T_{M1}: $\frac{\mathrm{d}M_1}{\mathrm{d}t}$ (gray), T_{M1} (dotted), total torque applied to the atmosphere T_{t1} (dashed) and ΩM_{r2} (mixed)

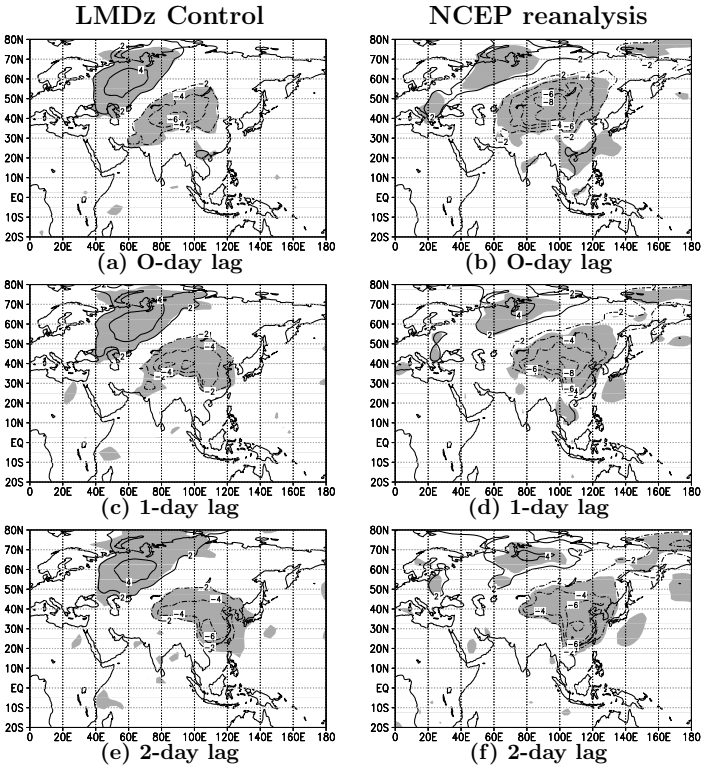

FIG. 4. 50m-temperature composites keyed to T_{t1}^{TP} from the REF simulation (left column) and from the NCEP reanalysis (right column). Panels in the first, second and third lines are for D0, D+1 and D+2 lags respectively. Contour intervals: 2K, zero contour is omitted, 99% significance levels are shaded.

differences on $\mathbf{T}_t$ or $\mathbf{M}_r$ result in large error on the much smaller tendency $\frac{d\mathbf{M}}{dt}$. In models, these errors can come from the dynamical core, as discussed for instance in Lebonnois et al. (2010) and Lauritzen et al. (2014) for the axial angular momentum. In this respect, it is noticeable that LMDz is a discrete model, using an Arakawa-C grid, the advection is Eulerian and explicit, properties that permit the equations to be discretized in order that mass and zonally symmetric angular momentum can be conserved (Hourdin 1992). Beyond these aspects, there are many other processes that can produce sources and sinks of AAM, like horizontal diffusion, but over the years they have been included or changed in LMDz keeping in mind that the model should conserve well the axial AAM. The motivation is that this model is intensively used to simulate the circulations of super-rotating atmospheres, an issue where the conservation of axial AAM is central (Lebonnois et al. 2010). We therefore found here that these efforts to conserve the axial component of the AAM benefit to its equatorial components as well.

Now, when it comes to re-analysis products, errors due to the assimilation or from the post-processing of the datas can add to model errors. Concerning the post processing Feldstein (2006) mentioned that daily averaging of data could be a cause, but our results also use daily data so this does not seem to be a major issue. On the contrary, we know from Graversen et al. (2007) that data assimilation affects the representation of the mass and energy budget in the ERA-40 reanalysis. More specifically, they show that during the assimilation, observations reset the surface-pressure field whereas the mass fluxes are not adjusted properly. In other words, the surface pressure can be very accurate in the reanalysis, but the mass transport can be in substantial error. This is because surface pressure observations are plentiful and accurate, in contrast to wind observations. For all these reasons, it is therefore not a surprise that the EAAM in LMDz is better closed here than in reanalysis products.

To analyze further the contribution of the torques to the atmospheric dynamics, we next follow Mailler and Lott (2010), which have shown that the EMT vector rotates counter-clockwise in the equatorial plane, with a rotation period of a few days. They also found that this global behaviour is in part a result of regional contributions where the cold surges contribute substantially. These results suggest that a regional approach is a good way to understand the dynamical impact of mountains on the atmospheric circulation.

4. Tibetan Plateau

One of the central points made in Mailler and Lott (2010) is that when a high pressure anomaly is located

poleward of a given mountain massif X in the Northern Hemisphere (resp. Southern Hemisphere) it gives rise to a positive (resp. negative) regional mountain torque T^X_{M1}, and that this mountain torque in part controls the future evolution of the flow, triggering a cold surge, which then produces a negative (resp. positive) T^X_{M2}. As already said, the initial situation with high pressure to the north of the massif corresponds to a positive contribution to T^X_{M1} but also to a negative zonal wind in the lower troposphere over the mountains. Now, the SSO parameterization in Lott (1999) predicts from this negative wind a surface stress that is northward and thus produce a positive T^X_{l1} as well. The northward acceleration associated with it (in the NH) is equilibrated by a Corolis term with an ageostrophic positive zonal wind anomaly transporting masses from west to east which builds up a high pressure center to the east of the massif: it can also contribute to the cold surge (Mailler and Lott 2010). In this picture, the mountain torques, either explicit or parameterized, are key drivers of the cold surges but we need to address their relative role.

To test if the relation between equatorial torques and cold surges is at work in our model, Fig. 4 shows composites of the 50-m temperature keyed on the first component of the EMT due to the Tibetan Plateau T^{TP}_{t1}, and keeping the 30 largest maxima of T^{TP}_{t1} out of the 30-years considered: around one peak per year is selected, which ensures good independence between the dates selected to build the composites, so the significance of the results can be measured via a student t-test. We see that in both model and reanalysis, the peaks in T^{TP}_{t1} are associated with cold anomalies over and north of the Tibetan Plateau (8 K in NCEP, 6 K in LMDz), and to a warm anomaly in northwestern Siberia (Fig. 4a-b). At 1-day lag in Figs. 4c-d, the cold anomaly shifts towards the eastern slopes of the Tibetan plateau without losing intensity. This south-eastward displacement around the massif continues thereafter and at 2-day lag the cold anomaly reaches the subtropical latitudes: in both LMDz and NCEP the cold temperature signal is significant at 20°N at this time (Figs. 4e-f). Importantly, we see that the signals in LMDz and NCEP are very close at all lags and locations, witnessing that the relationship between the cold surges and the mountain torques is represented realistically in LMDz.

The corresponding composites of surface pressure in Fig. 5 corroborate those for the temperature. Without surprise, the peaks in T^{TP}_{t1} are due to a strong meridional pressure gradient over the Tibetan plateau, which is essentially related to a strengthening of the Siberian high (typically 14 hPa above its climatological value in both datasets). As for temperature, this high pressure system rotates southeastward around the plateau, yielding a configuration that is favourable to produce a negative T^{TP}_{t2}. Again, the maps are very similar between the datasets. The main difference between them is the apparition of a high pressure anomaly

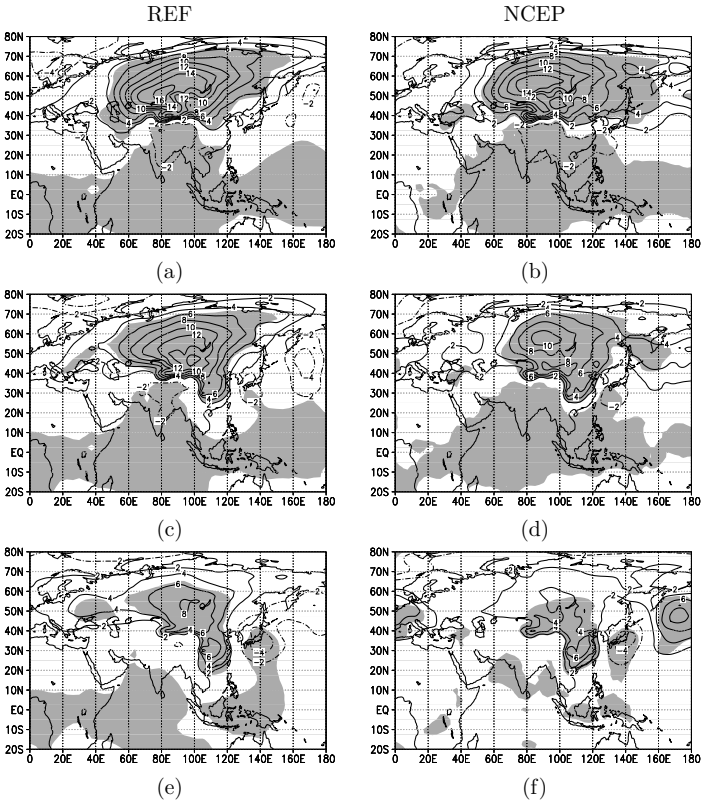

FIG. 5. Same as Fig. 4 but for the surface pressure. Contour interval: 2hPa.

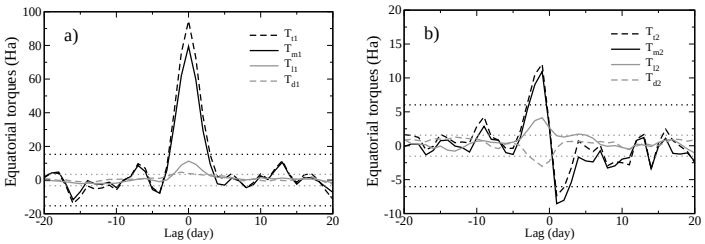

FIG. 6. LMDz composites of the different components of the EMT due to the Tibetan plateau, and keyed to T_{t1}^{TP}: a) First equatorial component, b) second equatorial component. For i=1,2: T_{ti}^{TP} (black dashed), T_{Mi}^{TP} (black solid), T_{li}^{TP} (grey), T_{di}^{TP} (grey dashed). The horizontal dotted lines are 1% significance levels for the total torque (black) and for the lift torque (grey).

in the Northern Pacific in NCEP, which does not appear with LMDz. Also, the persistence of the high pressure anomaly north of the TP at D+2 is somewhat stronger in LMDz than in NCEP.

The composites of the various torques due to the Tibetan plateau in Fig. 6a show that the major contribution comes from the explicit term T_{M1}^{TP}, but that there is a small contribution of the lift torque T_{l1}^{TP}. This contribution adds up around 19% to the explicit torque to build up the total torque. This is consistent with the purpose of these terms, which is to increase vortex stretching over the large-scale mountains by including the effect of subgrid-scale orography. The composites of the second components of the EMT in Fig. 6b show that this component is essentially in quadrature with the first, with a positive T_{M2}^{TP} in the few days that precede the peak in T_{M1}^{TP} and a negative T_{M2}^{TP} in the following few days. This general behaviour is also found in the NCEP data (not shown but see Fig. 4a in Mailler and Lott (2010)), and the negative T_{M2}^{TP} at positive lag are clearly related to the high pressure system present on the eastern slopes of the Tibetan plateau in Figs. 5c and 5e.

5. Rockies and Andes

For the Rockies, the composite of surface pressure keyed on maxima of the total torque T_{t1}^{R} are shown in Fig. 7. They are quite similar to what occurs over the Tibetan plateau, since at 0-day lag, the peak in T_{t1}^{R} is related with anomalies of high surface pressure over Alaska and the Arctic ocean, which extend eastward of the Rockies over the Canadian plain (Figs. 7a-7b). At this lag, the main difference between LMDz and NCEP is found over the Atlantic. The peak in T_{t1}^{R} at D0 in LMDz (Fig. 7a) and in NCEP (Fig. 7b) is explained by a strong high pressure anomaly north of the mountains and, to a lesser extent, a low pressure anomaly south of the mountains over the Northern

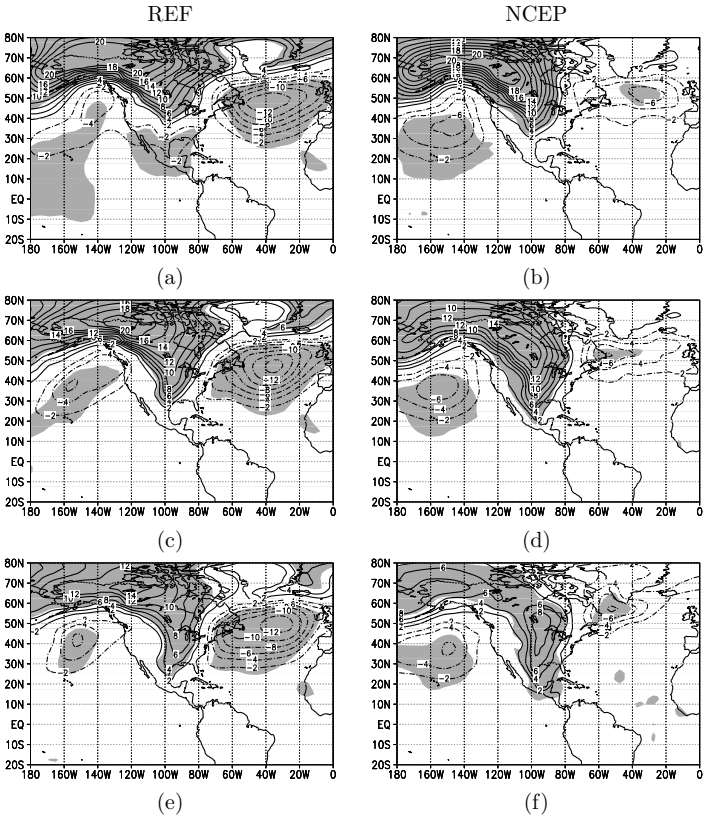

FIG. 7. Surface pressure composites for the Rockies in the NCEP dataset and in the REF simulation, for DO after the peak in T_{t1}^{R}(first line), D+1 (second line) and D+2 (third line). Contour interval: 2 hPa, zero-contour is omitted, shaded areas represent 1% significance.

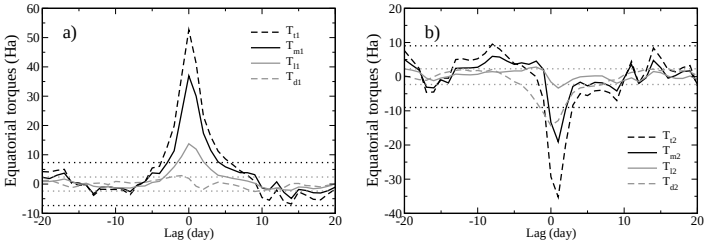

FIG. 8. Same as Fig. 6 but for the Rockies.

Pacific. These two datasets statistically show different signals over the northern Atlantic, with a very strong trough in the LMDz model which is much more attenuated in the NCEP reanalysis. However, these differences occur too far from the Rocky mountains for us to attribute it without ambiguity to an orographic effect. If we stay near the mountains, and regarding the temporal evolution of the cold surge in Figs 7c-d, the two datasets are consistent, with the low pressure anomaly moving southward in both. At an even later stage in Figs 7e-f, the cold surge penetrates well into the subtropics. The signal in the reanalysis there is stronger, but the model still has no major difficulties in reproducing the temporal development of the surface pressure anomaly toward the subtropics.

If we now return to the torques related to the evolution of the surface pressure in Fig. 8a, we see that for the Rockies also, the lift torque due to the SSO parameterization makes up a good part of the total torque (about 30%). Also, a negative peak in T_{t2}^R follows that in T_{t1}^R (Fig. 8b) and the model behaviour is consistent with the similar behaviour of the EMT components due to the Rockies in NCEP (Mailler and Lott 2010).

For the Andes, the location in the southern hemisphere makes that our composites must be keyed to negative values of the local torque T_{t1}^{Ad}, in order to allow comparison with the other massifs. For the surface pressure the composites from LMDz and NCEP in Fig. 9 show again that the model is quite realistic. At 0-day lag the negative torque T_{t1}^{Ad} is related to an anticyclonic circulation pattern centred on the southern tip of South America. This anticyclonic circulation develops at further stages to cover the eastern flank of the Andes, up to the subtropics again. In the NCEP data, this eastward development is associated with a weakening of the initial high, whereas in the model, an anomalous high pressure signal persists at the southern tip of the continent (see Figs. 9e-9f). As we will see next, this is probably due to an overestimation of the torques due to the SSO parameterizations in the southern part of the Andes.

The possibility that the torque due to the SSO is overestimated in the reference simulation is illustrated by Fig. 10a which shows the composite of the first components of the EMT due to the Andes. In it we see that the negative peaks

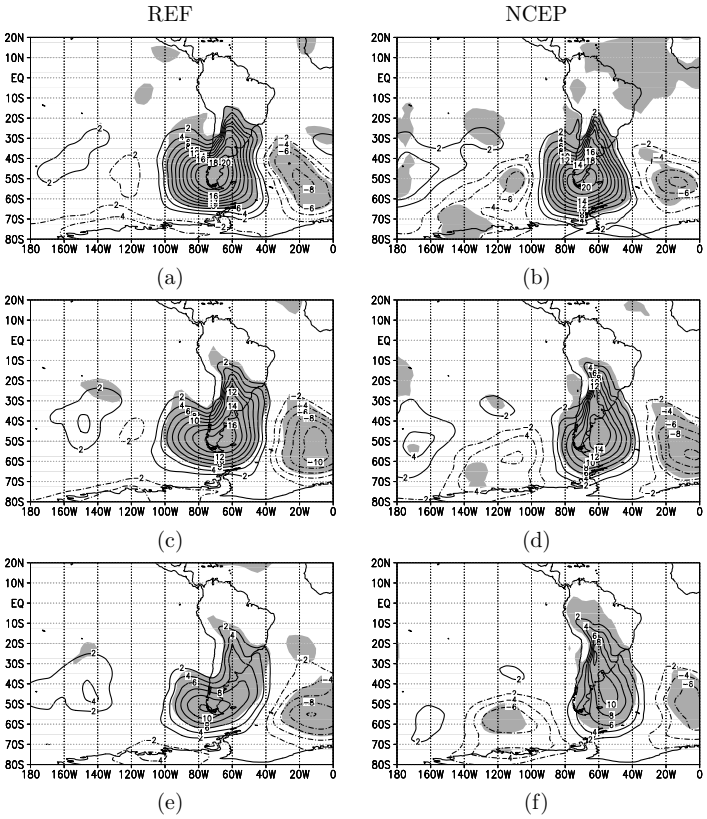

FIG. 9. Surface pressure composites keyed to T_{t1}^{Ad} in the NCEP dataset and in the REF simulations, for DO (first line), D+1 (second line) and D+2 (third line)

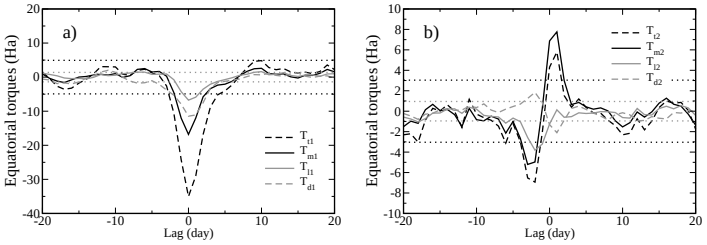

FIG. 10. Same as Fig. 6 but for the Andes.

in the explicit mountain torque are about −15Ha, which is quite comparable to what was found in the NCEP reanalysis in Mailler and Lott (2010). Nevertheless the total torque is about two times larger, and the difference essentially comes from the drag parameterization through T_{d1}^{Ad}. When we sum up this terms to the lift term T_{l1}^{Ad}, we see that half of the torque comes from the parameterizations rather than from the explicitly mountain torque T_{M1}^{Ad}. We will see in the next section that when this parameterized contribution is reduced, the signal actually improves over the southern part of South America. Following the peak in T_{t1}^{Ad}, there is a rapid increase of 15 Ha in the second component of the torque T_{t2}^{Ad}, and this is true for the mountain torque as well as for the total torque (see Fig. 10b). This increase is consistent with that found in the NCEP reanalysis in Mailler and Lott (2010), and is a natural consequence of the fact that the development of the ridge along the eastern flank of the model is quite realistic in LMDz (Fig 9e,f).

6. Impact of the SSO parameterizations

The fact that the LMDz GCM reproduces well the cold surges and the relationship between the mountain forcing and the cold surges suggest that our composite techniques can be used to evaluate the impact of parameterization of SSO in models. To illustrate this point, the right panels in Fig. 11 shows composites of surface pressure at 2-day lag in the simulations where the SSO parameters have been set to zero over the corresponding mountain. For clarity we repeat on the left the composite keyed to the total torques in the reference simulation. The first striking result is that the impact is rather small, with the runs where the SSO parameterizations are active resulting in slightly stronger surface pressure signal than when the SSO parameterizations are not active. If we return to the mountain torques and for the Tibetan Plateau, the smallness of the difference is not surprising since the SSO torque only makes around 10% of the total torque in Fig. 6a. On top of that, it appears that in the run without SSO torques, the explicit torque partly compensates the deficit in parameterized torque (see Fig. 12a). In the end, if we follow the linear formulation of Mailler and Lott (2010), the largest signal one can expect of such differences can only be of 1-2 hPa, and this is typically the maximum difference we found between the composites in Figs. 11a–11b.

For the Rockies, the compensation of the SSO torques by an increase of the explicit torque is not as pronounced as over the Tibetan Plateau but still present (see Fig. 12b). Without surprise, the differences in the composite are more pronounced, the control run has a stronger cold surge signal immediately in the lee of the Rockies, but again, the differences are small and only marginally significant (see Figs. 6c and 6d). For both the Tibetan Plateau and the Rockies, we noticed in Figs. 6a and 8a that the SSO scheme

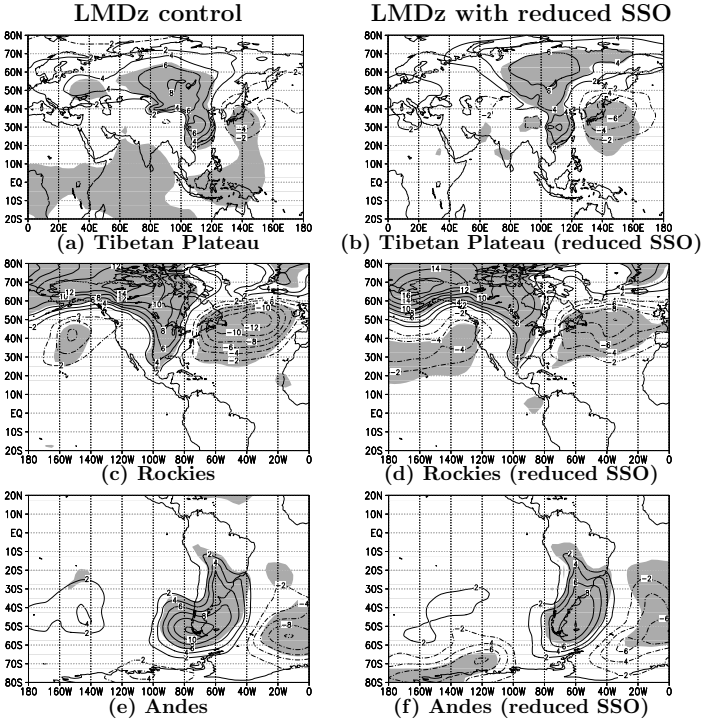

FIG. 11. Composite of surface pressure anomaly at D+2 after the peaks of the T_1 for the Tibetan Plateau (first line), the Rockies (second line) and the Andes (third line). The left column shows the composites in the control simulation, the right column shows the composites when subgrid-scale orography is suppressed over the considered mountain range (Tibetan Plateau for 11b, Rockies for 11d, Andes for 11f). Contour interval is 2 hPa, zero-contour is omitted, shaded areas represent 1% significance

that enhances the first component of the equatorial mountain torque is essentially the lift force introduced in Lott (1999). We therefore see here that changing this term can affect the cold surges, and eventually increase their amplitude. When it comes to the Andes, we have noticed that the SSO torques play a much more substantial role, building up almost 50% of the total torque, the additional torque being essentially due to the SSO drag rather than to the SSO lift (see Fig. 10a). In this case, and with the additional torques the surface pressure composite is much larger in the control run than when there is no SSO parameterization, as for the other massifs, but much less in error when compared to the NCEP composites in Fig. 9f). This suggests that the SSO drag does not necessarily improve the cold surge, as the SSO lift seemingly does for the other mountains. This is consistent with the arguments in Lott (1999) about the reduction of model errors by lift forces rather than by drag forces and confirms that both components should be analyzed and tuned.

7. Conclusion and discussion

This paper shows that the EAAM budget is much better closed in the LMDz GCM than in reanalysis datasets. Compared to the axial budgets analyzed for instance in Lott et al. (2001, 2008), the main difficulty is that the equatorial budget equations includes two large terms that almost cancel each other, the mountain torque and the Coriolis term, and that the difference between these terms drives the evolution of the equatorial AAM. Small relative errors on these two terms can therefore result in large errors in the prediction of the evolution of the EAAM. As this problem is largely alleviated in the LMDz GCM we have more confidence in the interpretation of the evolution terms. This permits us to confirm the finding of Feldstein (2006) that the EAAM evolution is dominated by 8-10 days periods associated with planetary scale waves.

The use of model data from LMDz with a verified closure of the EAAM budget strengthens the results about the relations between mountain torques and cold surge triggering that have been found in Mailler and Lott (2010). Confirming what was found in reanalysis data, we find that in the model, peaks in the component of the local EMT vector pointing toward the closest pole are followed by the development of intense cold surges a couple of days later. As this result is based on a composite analysis, it tells us that models can simulate well the pre-conditioning phase of cold surges, providing that they simulate their synoptic precursor, e.g. that they predict well the occurrence of anti-cyclonic anomalies poleward of large-scale mountain massifs. In these relations between the mountain torques and the synoptic development of the cold surges, the analysis indicates that the parameterized torques play a substantial role, contributing between 10% and 50% to the

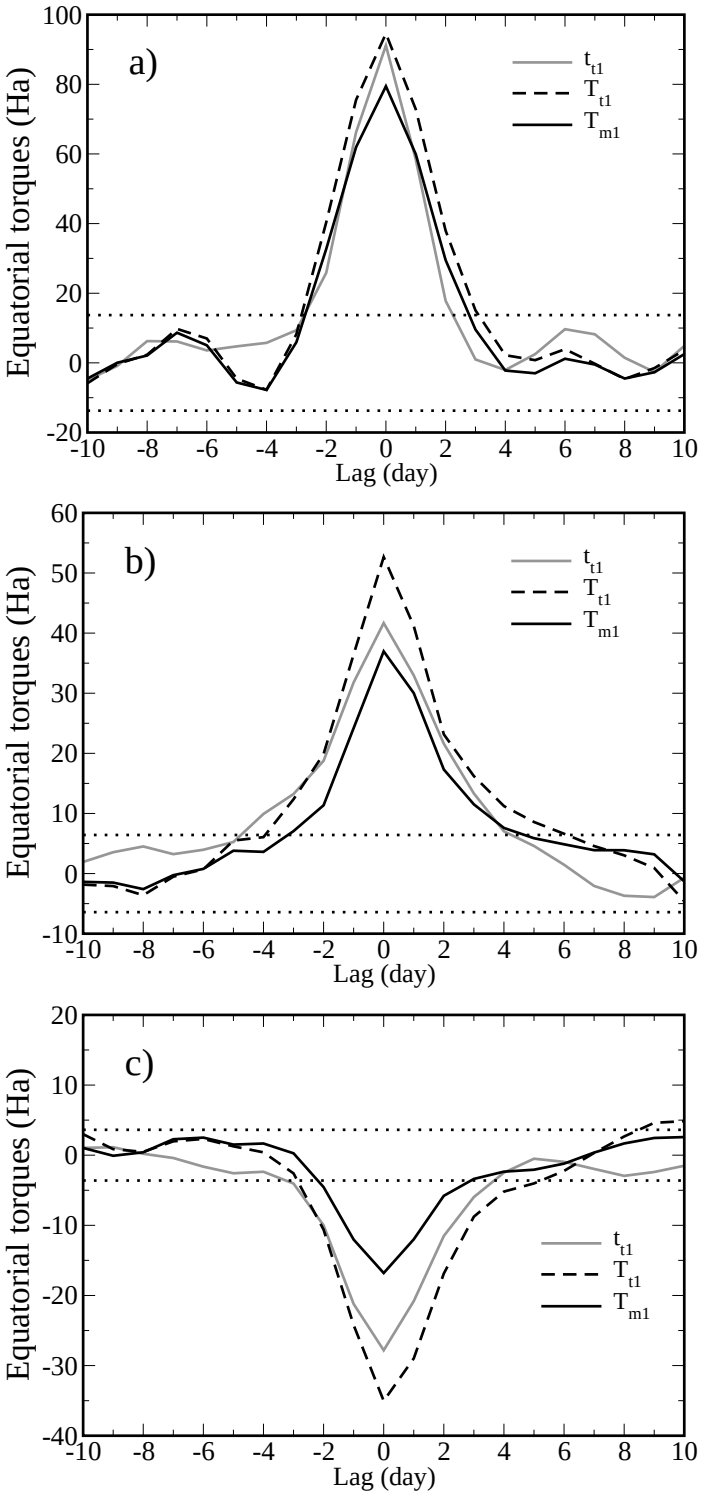

FIG. 12. First components of the EMT in the runs with and without SSO parameterizations. a) Tibetan Plateau torques, b) Rockies torque, and c) Andes torques. In all panel, the explicit and total torques (T_{m1} and T_{t1}) are from the control run whereas the total torques t_{t1} are from the run without SSO parameterization.

regional EMT contributions due to the Tibetan Plateau, the Rockies and the Andes.

The significance of the contribution of the parameterized torques is also confirmed by three numerical experiments, where the parameterized torques are suppressed for each of the three massifs we have considered. The most striking result is that in these experiments, the contribution of the explicit torque increases so the effect on the cold surge is less pronounced than suggested by just analyzing the contribution of the parameterized torques to the total torques in the control experiment. Still, some differences occurs, and the control simulation has slightly more intense signals after the peaks in the torques than in the simulations without SSO parameterizations. Also, it seems that when the SSO lift is increased, the impact on the surges is beneficial in the case of the Tibetan Plateau and the Rockies. On the contrary, in the case of the Andes, it is the SSO drag that makes the largest contribution to the parameterized torques, and in this case, the control seems more in error regarding the surge than the experiment with reduced SSO drag.

For modellers, these results are good news since they tell that synoptic-scale phenomena affected by mountains, like the cold surges, are not very sensitive to the details of the SSO parameterizations. A clear message is nevertheless that in the SSO schemes, all components of the mountain force with respect to the direction of the wind should be taken into account: changing the direction of the large scale flow is not equivalent to decelerating it, as it is confirmed here for the case of the cold surges. Nevertheless, the substantial increase of the explicit mountain torque when the SSO parameterizations are reduced shows that much longer and refined tests should be done to address the effects of SSO parameterizations on synoptic scale flows.

From a more fundamental point of view, the compensation of the parameterized torques by explicit torques shows that the latter can be viewed as dynamical drivers of the large scale flow: if we suppress a term explicitly acting on the right hand side of the momentum equations, such as when the SSO parameterizations are suppressed, the explicit torque in part raises to compensate.

Acknowledgments.

This work was supported by the franco-argentinian ECOS program DIAGAC and by the french LEFE project DIAC. The authors are very grateful to Carolina Vera and Alejandro Godoy for useful discussions as well with Lionel Guez for technical assistance.

REFERENCES

Aebischer, U. and C. Schar, 1998: Low-level potential vorticity and cyclogenesis to the lee of the Alps. *J. Atmos. Sci.*, **55**, 186207.

Belcher, S. and N. Wood, 1996: Form and wave drag due to stably stratified turbulent flow over low ridges. *Q. J. R. Meteorol. Soc.*, **122**, 863–902.

Bell, M. J., 1994: Oscillations in the equatorial components of the atmosphere's angular momentum and torques on the earth's bulge. *Q. J. R. Meteorol. Soc.*, **120**, 195–213.

Chen, T.-C., M.-C. Yen, W.-R. Huang, and W. A. Gallus, 2002: An east-asian cold surge : Case study. *Mon. Weather Rev.*, **130**, 2271–2290.

Colle, B. A. and C. Mass, 1995: The structure evolution of cold surges east of the Rocky Mountains. *Mon. Weather Rev.*, **123**, 2577–2610.

Compo, G. P., G. N. Kiladis, and P. J. Webster, 1999: The horizontal and vertical structure of east asian winter monsoon pressure surges. *Q. J. R. Meteorol. Soc.*, **125**, 29–54.

De Viron, O., G. Schwarzbaum, F. Lott, and V. Dehant, 2005: Diurnal and subdiurnal effects of the atmosphere on the Earth rotation and geocenter motion. *J. Geophys. Res.*, **110**, B11 404, doi:10.1029/2005JB003761.

Dufresne, e. a., J-L, 2013: Climate change projections using the IPSL-CM5 Earth System Model: from CMIP3 to CMIP5. *Climate Dynamics*, **40**, 2123–2165, doi:10.1007/s00382-012-1636-1.

Egger, J. and K.-P. Hoinka, 2002: Equatorial components of global atmospheric angular momentum: Covariance functions. *Q. J. R. Meteorol. Soc.*, **128**, 1137–1157.

Egger, J., K. Weickmann, and K.-P. Hoinka, 2007: Angular momentum in the global atmospheric circulation. *Rev. Geophys.*, **45**, RG4007, doi:10.1029/2006RG000213.

Espinoza, J. C., J. Ronchail, M. Lengaigne, N. Quispe, Y. Silva, M. L. Bettolli, G. Avalos, and A. Llacza, 2012: Revisiting wintertime cold air intrusions at the east of the Andes: propagating features from subtropical Argentina to Peruvian Amazon and relationship with large-scale circulation patterns. *Clim. Dyn.*, doi:10.1007/s00382-012-1639-y.

Feldstein, S. B., 2003: The dynamics associated with equatorial atmospheric angular momentum in an aquaplanet GCM. *J. Atmos. Sci.*, **60**, 1822–1834.

Feldstein, S. B., 2006: Dynamical processes of equatorial atmospheric angular momentum. *J. Atmos. Sci.*, **63**, 565–581, doi:10.1175/JAS3586.1.

Garreaud, R. D., 1999: Cold air incursions over subtropical and tropical south america: A numerical case study. *Mon. Weather Rev.*, **128**, 2823–2853.

Garreaud, R. D., 2000: Cold air incursions over subtropical South America: Mean structure and dynamics. *Mon. Weather Rev.*, **128**, 2544–2559.

Garreaud, R. D., 2001: Subtropical cold surges: regional aspects and global distribution. *Int. J. Climatol.*, **21**, 1181–1197.

Giorgi, F., C. Jones, and G. R. Asrar, 2009: Addressing climate information needs at the regional level: the CORDEX framework. *WMO Bulletin*, **58 (3)**, 175–183.

Graversen, R. G., E. Kallen, M. Tjernstrm, and H. Krnich, 2007: Atmospheric mass-transport inconsistencies in the era-40 reanalysis. *Quarterly Journal of the Royal Meteorological Society*, **133 (624)**, 673–680, doi:10.1002/qj.35, URL `http://dx.doi.org/10.1002/qj.35`.

Hourdin, F., 1992: Conservation du moment cinetique dans le modele de circulation generale du lmd. *Note Interne LMD*, **175**, URL `http://lmdz.lmd.jussieu.fr/developpeurs/notes-techniques/ressources/conserv.pdf`.

Hourdin, F., et al., 2006: The lmdz general circulation model: climate performance and sensitivity to parametrized physics with emphasis on tropical convection. *Clim. Dyn.*, **27**, 787–813, doi:10.1007/s00382-006-0158-0.

Hsu, H.-H. and J. M. Wallace, 1985: Vertical structure of wintertime teleconnection patterns. *J. Atmos. Sci.*, **42**, 1693–1710.

Jeong, J.-H. and C.-H. Ho, 2005: Changes in occurrence of cold surges over east asia in association with arctic oscillation. *Geophys. Res. Lett.*, **32**, L14 704, doi:10.1029/2005GL023024.

Jeong, J.-H., C.-H. Ho, B.-M. Kim, and W.-T. Kwon, 2005: Influence of the madden-julian oscillation on wintertime surface air temperature and cold surges in east asia. *J. Geophys. Res.*, **110**, D11 104, doi:10.1029/2004JD005408.

Kalnay, E., et al., 1996: The NCEP/NCAR 40-year reanalysis project. *Bull. Am. Meteorol. Soc.*, **77**, 437–471.

Konrad II, C. E., 1996: Relationships between the intensity of cold-air outbreaks and the evolution of synoptic and planetary-scale features over north america. *Mon. Weather Rev.*, **124**, 10671083.

Lauritzen, P. H., J. T. Bacmeister, T. Dubos, S. Lebonnois, and M. A. Taylor, 2014: Held-Suarez simulations with the community atmosphere model spectral element (CAM-SE) dynamical core: A global axial angular momentum analysis using eulerian and floating lagrangian vertical coordinates. *J. Adv. Model. Earth Syst.*, doi:10.1002/2013MS000268.

Lebonnois, S., F. Hourdin, V. Eymet, A. Crespin, R. Fournier, and F. Forget, 2010: Superrotation of venus' atmosphere analyzed with a full general circulation model. *Journal of Geophysical Research: Planets*, **115 (E6)**, n/a–n/a, doi:10.1029/2009JE003458, URL `http://dx.doi.org/10.1029/2009JE003458`.

Li, W. and R. Fu, 2006: Influence of cold air intrusions on the wet season onset over Amazonia. *J. Clim.*, **19**, 257–275.

Lott, F., 1995: Comparison between the orographic response of the ECMWF model and the PYREX 1990 data. *Q. J. R. Meteorol. Soc.*, **121**, 1323–1348.

Lott, F., 1999: Alleviation of stationary biases through a mountain drag parameterization scheme and a simple representation of mountain lift forces. *Mon. Weather Rev.*, **127**, 788–801.

Lott, F., O. de Viron, P. Viterbo, and F. Vial, 2008: Axial atmospheric angular momentum budget at diurnal and subdiurnal periodicities. *J. Atmos. Sci.*, **65**, 156–171.

Lott, F., L. Goudard, and A. Martin, 2005: Links between the mountain torque and the Arctic Oscillation in the Laboratoire de Météorologie dynamique (LMDz), general circulation model. *J. Geophys. Res.*, **110**, D22 107, doi:10.1029/2005JD006073.

Lott, F., J. Kuttippurath, and F. Vial, 2009: A climatology of the gravest waves in the equatorial lower and middle stratosphere: Method and comparison between the era-40 re-analysis and the lmdz-gcm. *J. Atmos. Sci.*, **66**, 1327–1346.

Lott, F. and M. J. Miller, 1997: A new sub-grid scale orographic drag parameterization : Its formulation and testing. *Q. J. R. Meteorol. Soc.*, **123**, 101–127.

Lott, F., A. W. Robertson, and M. Ghil, 2001: Mountain torques and atmospheric oscillations. *Geophys. Res. Lett.*, **28**, 1207–1210.

Mailler, S. and F. Lott, 2009: Dynamical influence of the Tibetan Plateau on winter monsoon convection over southeast Asia. *Geophys. Res. Lett.*, **36**, L06708, doi:10.1029/2008GL036952.

Mailler, S. and F. Lott, 2010: Equatorial mountain torques and cold surges preconditionning. *J. Atmos. Sci.*, doi: 10.1175/2010JAS3382.1.

Marengo, J., T. Ambrizzi, G. Kiladis, and B. Liebmann, 2002: Upper-air wave trains over the pacific ocean and wintertime cold surges in tropical-subtropical south america leading to freezes in southern and southeastern brazil. *Theoretic. App. Climatol.*, **73**, 223–242.

Marengo, J., C. A. Nobre, and A. D. Culf, 1997: Climatic impacts of "friagens" in forested and deforested areas of the Amazon Basin. *J. Appl. Meteorol.*, **36**, 1553–1566.

Martin, A. and F. Lott, 2007: Synoptic responses to mountain gravity waves encoutering directional critical levels. *J. Atmos. Sci.*, **64**, 828–848, doi:10.1175/JAS3873.1.

Park, T.-W., C.-H. Ho, and S. Yang, 2011: Relationship between the arctic oscillation and cold surges over east asia. *J. Clim.*, **24**, 68–83, doi:10.1175/2010JCLI3529.1.

Park, T.-W., C.-H. Ho, S. Yang, and J.-H. Jeong, 2010: Influences of arctic oscillation and madden-julian oscillation on cold surges and heavy snowfalls over korea: A case study for the winter of 20092010. *J. Geophys. Res.*, **115**, D23 122, doi:10.1029/2010JD014794.

Pérez García, I., 1996: Major cold air outbreaks affecting coffee and citrus plantations in the eastern and northeastern Mexico. *Atmósfera*, **9**, 47–68.

Pezza, A. B. and T. Ambrizzi, 2005: Dynamical conditions and synoptic tracks associated with different types of cold surge over tropical south america. *Int. J. Climatol.*, **25**, 215–241, doi:10.1002/joc.1080.

Portis, D. H., M. P. Cellitti, W. L. Chapman, and J. E. Walsh, 2006: Low-frequency variability and evolution of North-American cold air outbreaks. *mwr*, **134**, 579–597, doi:10.1175/MWR3083.1.

Reason, C. J. C., 1994: Orographically trapped disturbances in the lower atmosphere: scale analysis and simple models. *Meteorol. Atmos. Phys.*, **53**, 131–136.

Schultz, D. M., W. E. Bracken, and L. F. Bosart, 1998: Planetary- and synoptic-scale signatures associated with central american cold surges. *Mon. Weather Rev.*, **126**, 5–27.

Schultz, D. M., W. E. Bracken, L. F. Bosart, G. J. Hakim, M. A. Bedrick, M. J. Dickinson, and K. R. Tyle, 1997: The 1993 superstorm cold surge: Frontal structure, gap flow, and tropical impact. *Mon. Weather Rev.*, **125**, 5–39.

Shafer, J. C. and W. J. Steenburgh, 2008: Climatology of strong intermountain cold fronts. *Mon. Weather Rev.*, **136**, 784–807.

Sprenger, M., O. Martius, and J. Arnold, 2013: Cold surge episodes over southeastern brazil a potential vorticity perspective. *Int. J. Climatol.*, **33**, 27582767, doi: 10.1002/joc.3618.

Vera, C. S. and P. K. Vigliarolo, 2000: A diagnostic study of cold-air outbreaks over South America. *Mon. Weather Rev.*, **128**, 3–24.

Woo, S.-H., B.-M. Kim, J.-H. Jeong, S.-J. Kim, and G.-H. Lim, 2012: Decadal changes in surface air temperature variability and cold surge characteristics over Northeast Asia and their relation with the Arctic Oscillation for the past three decades (1979-2011). *J. Geophys. Res.*, **117**, doi:10.1029/2011JD016929.

Zhang, Y., K. R. Sperber, and J. S. Boyle, 1997: Climatology and interannual variation of the east asian winter monsoon: results from the 1979-95 NCEP/NCAR reanalysis. *Mon. Weather Rev.*, **125**, 2605–2619.

Notation	Name	First axis (i=1)	second axis (i=2)
M_{ri}	Wind AAM	$\int a\rho\left(-u\sin\phi\cos\lambda+v\sin\lambda\right)dV$	$\int a\rho\left(-u\sin\phi\sin\lambda-v\cos\lambda\right)dV$
M_{mi}	Mass AAM	$\int -\frac{a^2\Omega}{g}p_s\sin\phi\cos\phi\cos\lambda dS$	$\int -\frac{a^2\Omega}{g}p_s\sin\phi\cos\phi\sin\lambda dS$
T_{Mi}	Mountain torque	$\int p_s\left(-\sin\lambda\frac{\partial h}{\partial\phi}+\cos\lambda\tan\phi\frac{\partial h}{\partial\lambda}\right)dS$	$\int p_s\left(+\cos\lambda\frac{\partial h}{\partial\phi}+\sin\lambda\tan\phi\frac{\partial h}{\partial\lambda}\right)dS$
T_{di}	Torque due to drag	$\int a\left(-\cos\lambda\sin\phi\,\tau_{d\lambda}+\sin\lambda\tau_{d\phi}\right)dS$	$\int a\left(-\sin\lambda\sin\phi\,\tau_{d\lambda}-\cos\lambda\tau_{d\phi}\right)dS$
T_{li}	Torque due to lift	$\int a\left(-\cos\lambda\sin\phi\,\tau_{l\lambda}+\sin\lambda\tau_{l\phi}\right)dS$	$\int a\left(-\sin\lambda\sin\phi\,\tau_{l\lambda}-\cos\lambda\tau_{l\phi}\right)dS$
Integrals:		$\int dS=\int_{-\pi/2}^{\pi/2}\int_0^{2\pi}a^2\cos\phi d\lambda d\phi$	$\int\rho dV=\int\int_0^{p_s}\frac{dp}{g}dS$

TABLE 1. Definitions of all the terms in the EAAM budget: $\tau_{d\lambda}$ and $\tau_{d\phi}$ are the zonal and meridional stresses due to the SSO and boundary layer drags, $\tau_{l\lambda}$ and $\tau_{l\phi}$ are the surface stresses related to the SSO "lift", a is the Earth radius, ρ the density, p_S the surface pressure, h the mountain height, u,v the zonal and meridional components of the wind, g the acceleration of gravity, λ the longitude and ϕ the latitude.